Heliyon 9 (2023) e22461

Contents lists available at ScienceDirect

Heliyon

journal homepage: www.cell.com/heliyon

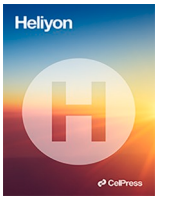

Cellular and molecular mechanisms of fibrosis and resolution in bleomycin-induced pulmonary fibrosis mouse model revealed by spatial transcriptome analysis

Qingsong Li [a,†], Yue Wang [a,†], Liu Ji [b,†], Jianhan He [c,†], Haixia Liu [a], Weizhen Xue [a], Huihui Yue [c], Ruihan Dong [c], Xin Liu [a,**], Daqing Wang [b,***], Huilan Zhang [c,1,*]

[a] *BGI-Beijing, Beijing 102601, China*
[b] *Dalian Maternal and Child Health Hospital of Liaoning Province, Dalian 116033, China*
[c] *Department of Clinical Research Center, Tongji Hospital, Tongji Medical College, Huazhong University of Sciences and Technology, Wuhan, Hubei, China*

ARTICLE INFO

Keywords:
Bleomycin-induced pulmonary fibrosis
spatial transcriptome
Self-resolving

ABSTRACT

The bleomycin-induced pulmonary fibrosis mouse model is commonly used in idiopathic pulmonary fibrosis research, but its cellular and molecular changes and efficiency as a model at the molecular level are not fully understood. In this study, we used spatial transcriptome technology to investigate the cellular and molecular changes in the lungs of bleomycin-induced pulmonary fibrosis mouse models. Our analyses revealed cell dynamics during fibrosis in epithelial cells, mesenchymal cells, immunocytes, and erythrocytes with their spatial distribution available. We confirmed the differentiation of the alveolar type II (AT2) cell type expressing *Krt8*, and we inferred their trajectories from both the AT2 cells and club cells. In addition to the fibrosis process, we also noticed evidence of self-resolving, especially to identify possible self-resolving related genes, including *Prkca*. Our findings provide insights into the cellular and molecular mechanisms underlying fibrosis resolution and represent the first spatiotemporal transcriptome dataset of the bleomycin-induced fibrosis mouse model.

1. Introduction Background

Idiopathic pulmonary fibrosis (IPF) is a chronic and progressive lung disease with unknown etiology, affecting approximately five million people and has few treatment options, resulting in a low 5-year survival rate of about 20 % [1,2]. Although the histological features of IPF, such as honeycomb cysts, fibroblastic foci, and hyperplastic epithelial cells, as well as molecular changes such as excessive accumulation of extracellular matrix (ECM), are well-known, the detailed cellular and molecular level changes in lungs during IPF are still under investigation [3]. Recent studies have applied cutting-edge single-cell sequencing technologies to illustrate

* Corresponding author.
** Corresponding author.
*** Corresponding author.
E-mail addresses: liuxin@genomics.cn (X. Liu), lnwangdaqing@126.com (D. Wang), huilanz_76@163.com (H. Zhang).
† These authors contributed equally.
1 Lead Contact.

https://doi.org/10.1016/j.heliyon.2023.e22461
Received 27 May 2023; Received in revised form 10 November 2023; Accepted 13 November 2023
Available online 20 November 2023

the pathogenesis of IPF in human [4–6], but animal models are important for understanding the pathological process and for developing drugs and treatments [3]. Bleomycin-induced pulmonary fibrosis mouse model is a widely used experimental model for studying IPF. The model is induced by intratracheal instillation of bleomycin, a chemotherapeutic agent that causes lung injury and fibrosis [7]. The model has been used to investigate the cellular and molecular mechanisms underlying the pathogenesis of IPF [8–10], as well as to evaluate the efficacy of potential therapeutic agents [11–13]. Despite its acuteness and self-resolving nature, the bleomycin injection mouse model has been comprehensively studied in different levels to reveal its pathogenic process [14,15]. Intracellular hydroxyproline content was comprehensively studied in the bleomycin injection-induced mouse lung fibrosis model over time to reveal the contradictory changes in hydroxyproline content along fibrosis and self-resolving processes [14]. Single-cell studies on the mouse model revealed major cellular changes, particularly one transitional cell type between AT1 and AT2 cells expressing *Krt8*, to be critical for lung fibrosis [15]. Further studies on the bleomycin-induced mouse model should provide more details on the essential process of pulmonary fibrosis and, more importantly, prove its efficiency as an IPF model.

Studies focusing on familial pulmonary fibrosis or genome-wide association studies have identified genetic factors related to idiopathic pulmonary fibrosis (IPF), including genes related to mucin production (*MUC5B* and *MUC2*) [16,17], surfactant proteins (e.g., *SFTPC*) [18], ER stress, and DNA repair. *MUC5B* has been identified as one of the marker genes for IPF in humans, with correlations to lung function, disease progression, and treatment responses [19,20]. Exploring the expression patterns of these known IPF-associated genes in the bleomycin-induced mouse model can improve our understanding of molecular-level changes during mouse lung fibrosis and reveal the efficiency of the model. Spatial transcriptome technology, such as SpaTial Enhanced REsolution Omics-sequencing (Stereo-seq), provides spatial information and a large view of massive cells, making it effective for studying cellular and molecular changes during pathogenic processes [21–24].

In this study, we applied Stereo-seq technology to study the lungs of bleomycin mouse models, generating the first spatial transcriptome dataset of normal (control), acute fibrosis (7 days after bleomycin injection), and recovering from fibrosis (21 days after bleomycin injection) lungs. We analyzed the dataset to reveal changes in cell types and subtypes during fibrosis, reflecting the efficiency of this animal model. We also identified and analyzed gene expression changes along fibrosis to confirm previously known key factors and identify possible genes related to the self-resolving feature.

2. Materials and methods

2.1. The bleomycin instillation induced mouse model

WT C57BL/6 mice were anesthetized with 1 % pentobarbital sodium (60 mg/kg) and then intratracheally administered BLM (1.8U/kg, Cat#HY-17565A/CS-0131163) in 50 μl of normal saline. Mice administered with same volume of normal saline served as controls. The mice were euthanized on day 7 and 21 following BLM challenge to analyze PF. All mice were housed in a specific pathogen-free (SPF) facility at the Tongji Medical College with a 12-h light/12-h dark cycle.

2.2. Sample preparation and sequencing

Mice were collected, and their lungs were excised for cryosectioning. The lungs were positioned correctly using a blunt metal needle, and once the OCT compound solidified on a flat surface of a dry ice block, cryosections were obtained at a thickness of 15 μm using a Leica CM1950 cryostat.

The STOmics Gene Expression kit S1 (BGI, 1000028493) was utilized according to the standard protocol V1.1 with minor modification [21]. Tissue sections were adhered to the Stereo-seq chip, and incubated in −20 °C methanol for 30 min fixation, followed by nucleic acid dye staining (Thermo fisher, Q10212) and imaging (Ti-7 Nikon Eclipse microscope). For permeabilization, tissue sections were permeabilized at 37 °C for 5 min. The cDNA was purified using AMPure XP beads (Vazyme, N411-03). The indexed single-cell RNA-seq libraries were constructed according to the manufacturer's protocol. The sequencing libraries were quantified by Qubit ssDNA Assay Kit (Thermo Fisher Scientific, Q10212). DNA nanoballs (DNBs) were loaded into the patterned Nano arrays and sequenced on MGI DNBSEQ-Tx sequencer (50 bp for read 1, 100 bp for read 2).

2.3. Binning data of spatial stereo-seq data

Raw data were processed according to a publicly available pipeline SAW available at https://github.com/BGIResearch/SAW. Transcripts obtained from 50 × 50 DNBs were merged as one bin 50 (~25 μm). In order to ensure each unit has a sufficient number of genes to respond to its molecular characteristics, we considered a single bin 50 as the fundamental analysis unit, according to previous work [21]. Bin IDs were synthesized based on their spatial coordinates (spatial_x and spatial_y) on the capture chip. Specifically, we selected the DNB located at the bottom-left corner of bin 50 to represent the location of the entire bin. To ensure data quality, we chose 201 genes, 251 genes, and 351 genes as the filtering thresholds for 0d, 7d, and 21d samples, respectively, and excluded any bin50 with a lower gene count than this value. The filtering thresholds were determined based on the gene count distribution curve of per bin 50; low-quality bin 50 would be clustered into a small peak, and we chose the lowest value to the right of the small peak as the filtering threshold.

2.4. Cell clustering and annotation

Data normalization, scaling, and bins clustering were processed using the R package Seurat (version 4.3.0) [25]. The function 'SCTransform' was used to normalize, scale, and merge different data sets for each time point. We identified the 3000 high variable features using 'VariableFeatures' function for each time point and then use them to perform dimensionality reduction by PCA and UMAP embedding. The cells were clustered using 'FindNeighbors' function using the first 30 principal components, followed by 'FindClusters' function. Marker genes of different clusters were found by 'FindAllMarkers' of Seurat R package, with parameter (min.pct = 0.1, logfc.threshold = 0.25) and filtered by pvalue.adj <0.05. Cell identities of clusters were annotated using marker genes. All cell clusters were identified by using known cell type–specific markers for each cluster. To get more detailed cell types, bins belonging to a specific cell type, or groups of relevant cell types were further clustered and annotated. The process of subcluster annotation for one cell type just like above description of cell type.

2.5. Cell chat (Ligand-receptor analysis)

We perform inference, analysis and visualization of cell-cell communication network for spatial imaging dataset using CellChat (version 1.6.1) [26] package. Initially, we created a new CellChat object from our Seurat object for each time point, utilizing the CellChatDB.mouse database, which contains 2021 validated molecular interactions, including 60 % secreted autocrine/paracrine signaling interactions, 21 % extracellular matrix-receptor interactions, and 19 % cell-cell contact interactions.

We preprocessed the expression data by identifying over-expressed genes and interactions, and then used the 'computeCommunProb' and 'filterCommunication' functions to infer the cellular communication network and compute the communication probability. The 'computeCommunProbPathway' function was then used to calculate the communication probability on a signaling pathway level by summarizing the communication probabilities of all ligands-receptors interactions associated with each signaling pathway.

To obtain an aggregated view of the cell-cell communication network, we utilized the 'aggregateNet' function, which counted the number of links or summarized the communication probability for each communication pair. Finally, we merged the three CellChat objects of each time point by utilizing the 'mergeCellChat' function for downstream analysis.

2.6. Cell differentiation inference

The pseudotime trajectories were performed using Monocle2 (version 2.2.41) [27] package with default settings.The differential gene expression test along the cell trajectory was conducted using differentialGeneTest with the 'fullModelFormulaStr' was set to cell type and time point. To identify genes associated with trajectory differentiation, we filtered for genes with a q-value <0.01.

Afterwards, we performed lineage inference between AT and club using Monocle3 [28] package. Pseudotime heatmap showing the differentiation direction across different cell lineages, plotted using plot_cells function. To screen for genes driving epithelial cell differentiation, we utilized the Moran's I statistic in Monocle3. Briefly, we first performed dimensionality reduction and trajectory inference on the stereo-seq data using Monocle3's built-in functions. We then identified the genes that were significantly (qval <0.01) spatially autocorrelated along the trajectory using the Moran's I statistic, which measures the degree of similarity in gene expression between neighboring cells in the trajectory. The genes with a Moran's I value greater than 0 were retained as potential drivers of epithelial cell differentiation. Besides, we test genes for differential expression in club_*Bpifa1* based on the low dimensional embedding and the principal graph using graph_test function. In addition, we assessed gene co-expression in club$^{Bpifa1+}$ by utilizing the graph_test function on the low-dimensional embedding and principal graph of the stereo-seq data.

2.7. Differential gene expression (DEG) analysis and GO enrichment

DEG of the same cell type between two time points were performed using 'FindMarkers' functions in Seurat packages, filtering significant DEGs with an adjusted p-value <0.05 and an absolute average log2 fold change >1. To further analyze the functional implications of these genes, we performed GO enrichment analysis of the Biological Process category using the clusterProfiler (version 4.4.4) [29] software package, with gene annotations provided by the org.Mm.eg.db [30] annotation database for mouse loci.

2.8. Protein-protein interaction (PPI) network analysis of spatial modules

We used the Retrieval of Interacting Genes (STRING) database (version 11.0, https://string-db.org/) to explore potential protein-protein interactions. Our analysis consisted of all protein-protein interactions in the "Mus musculus" species, with active interaction sources based on co-expression analysis. We utilized STRING confidence scores, considering a score of at least 0.7 as significant, to assess reliability of the interactions. In these networks, the nodes correspond to the proteins and the line between two nodes represent the relative connectivity in each network.

2.9. Single-cell reference mapping

Single-cell reference mapping was performed using the 'TransferData' function from the R package Seurat [25]. A previously published single-cell dataset was utilized as the reference dataset to classify the query cells. FindTransferAnchors was applied as an

initial step in integrating single-cell data and spatial data, enabling the identification of shared gene expression patterns between two distinct datasets. Anchor points were created by identifying commonly expressed genes and used to eliminate differences between the datasets in subsequent integration analyses. Once a set of anchors was found between the reference and query object, the TransferData object was utilized to transfer data from the reference to the query object. The spatial dataset was used as the query object, and each cell was labeled with the predicted cell type with the highest prediction score.

2.10. Gene set enrichment analysis (GSEA)

Gene expression data were analyzed using the ssgsea algorithm, which calculates enrichment scores for predefined gene sets. Specifically, we employed the irGSEA (version 1.1.3) R package to estimate the changes in expression levels of known genes involved in pulmonary fibrosis. And show the expression and distribution of risk score in ssgsea among cell clusters using boxplot.

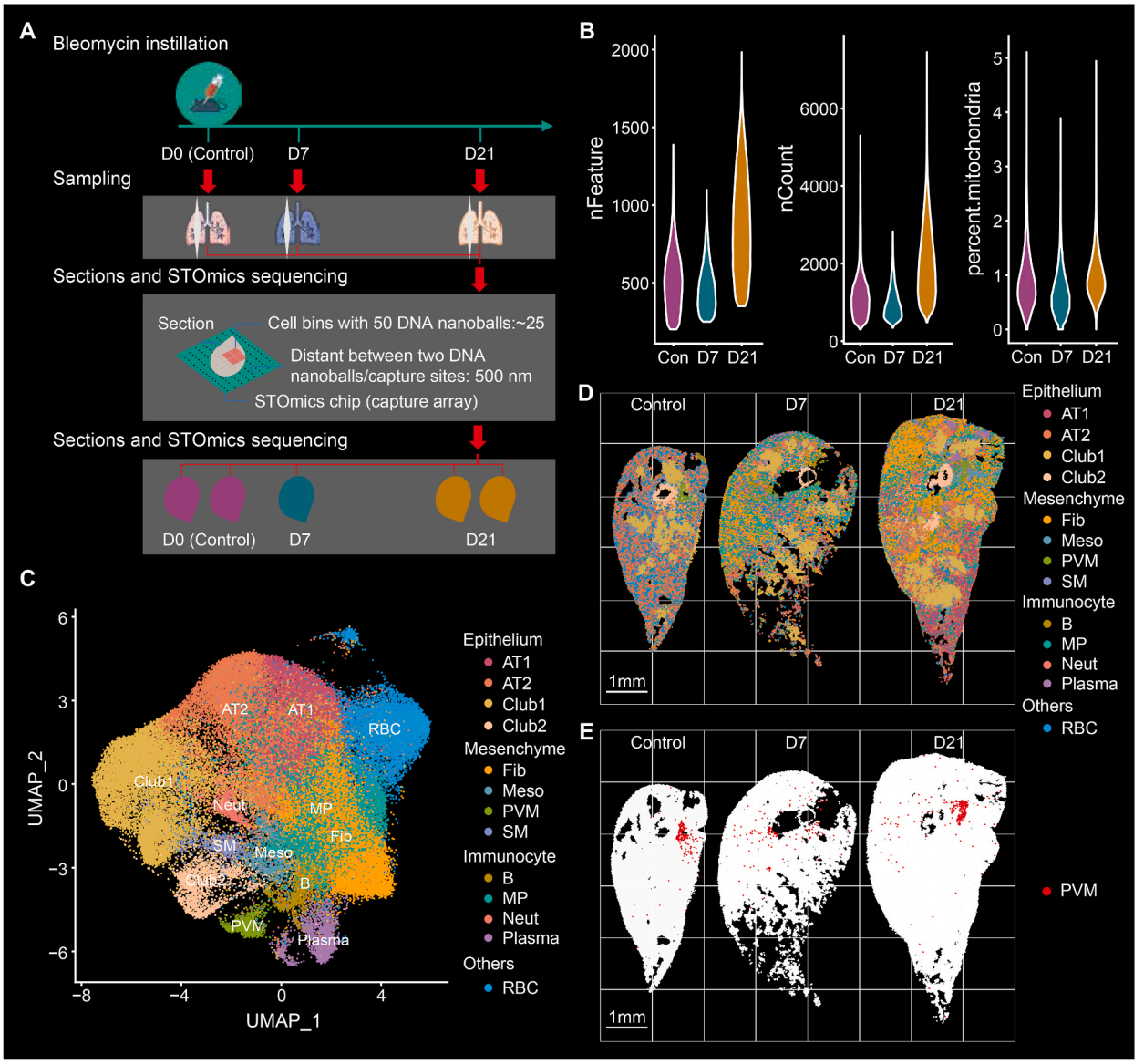

Fig. 1. Establishing a spatiotemporal transcriptome atlas of lungs from bleomycin induced pulmonary fibrosis mouse model. A, Schematic diagram of the experimental procedure and the whole study. **B**, Quality control of the cell bins to show their boxplots of nFeature (representing genes captured), nCount (RNA molecular captured) and percent.mt (percentage of the mitochondria) in the control lung (Con), the 7d lung (D7, 7 days after bleomycin instillation) and the 21d lung (D21, 21 days after bleomycin instillation). **C**, Uniform Manifold Approximation and Projection (UMAP) plot to show all the thirteen cells and their cell type annotation. **D**, Spatiotemporal distribution of the thirteen cell types. We showed one slice of each lung here and here after. **E**, Spatiotemporal distribution of PVM cells.

3. Results

3.1. Establish a spatial transcriptome atlas of lungs along fibrosis

To construct a spatiotemporal transcriptome atlas of the bleomycin instillation induced lung fibrosis mouse model, we obtained the spatial transcriptomes of lungs from 0 day (control), 7 days (D7) and 21 days (D21) after the bleomycin instillation (Fig. 1A). We obtained transcriptome data from five sections in total (two sections for control and 21d lungs and one section for 7d lung), with the total data amount of 699 Gbp. We followed previous described method [21], to define bins on the sections to represent cells (cell bins) and we set the bin size to be 50 nanoballs square (the nanoballs were the capture sites, and the actual size of these squares was ~25 μm). Filtering cell bins with insufficient number of genes captured (201 genes for control, 251 genes for 7d, and 351 genes for 21d), we obtained 77,687 cell bins in total, with 21,726, 13,439, and 42,522 cell bins for control, 7d and 21d lungs, respectively. The average number of genes in these defined cell bins was 713 and the average number of transcripts per cell bin was 1629 with maximum mitochondrial percentage to be 5.1 %, reflecting good gene expression capture efficiency (Fig. 1B).

Then, for all cell bins after normalization and standardization, we clustered and annotated them (Table 1). We first used previously reported marker genes, to annotate all these cell bins into four categories (epithelium, mesenchyme, immunocyte and red blood cells) and thirteen cell types, including alveolar type I (AT1) cells, alveolar type II (AT2) cells, club 1 cells, club 2 cells, fibroblast (FB), mesothelial cells (Meso), pulmonary vein myocardium (PVM), smooth muscle (SM) cells, B cells, macrophages (MP), neutrophil (Neut), plasma and red blood cells (RBC) (Fig. 1C). We further categorized twenty-eight clusters into thirteen cell types (Table 1), with marker genes to be identified and indicated. Our cell type annotation is comparable to recent single-cell studies, to have revealed major cell types in lungs [15,31], reflecting the effectiveness of the generated dataset.

Comparing to single cell sequencing data, the spatial transcriptomes also contain the cell location information, thus we were able to locate the cells on the slides with their spatial distributions shown (Fig. 1D). Using the spatial distribution information, we investigated one of the cell types we identified, PVMs, to reflect the advantage of spatial transcriptome data. PVMs were not commonly found and reported in previous single cell sequencing studies on lungs, probably because of limited capture efficiency or biased cell capturing, except one previous study [31], in which large amount of single cells were obtained and sequenced with Pericytes to be annotated. In our dataset, we found these cells to be in low proportion (1.22 %), and they distributed in concentrated regions in the upper lobe (Fig. 1E), which should be the vascular regions. The capture and annotation of PVMs in our dataset, again indicated high efficiency of our experiments in in situ capture and sequencing, as well as good quality of our dataset. To our knowledge, this is also the first spatiotemporal transcriptome atlas of mouse lungs, related to bleomycin injection and pulmonary fibrosis.

Table 1
Summary of the established spatiotemporal atlas.

Cluster	Marker gene	Cell type	Category	Cell number	Control	7d	21d
0	*Inmt, Sftpc, Hopx, Ager*	AT2	Epithelium	7544	5676	785	1083
1	*Timp1, Fn1*	Fibroblast	Mesenchyme	7135	100	2068	4967
2	*Cyp2f2, Scgb3a2*	Club1	Epithelium	6399	3008	1162	2229
3	*Hbb-bs, Hbb-a1, Hbb-a2, Hbb-bt*	Erythrocyte	RBC	6335	3377	1157	1801
4	*Col1a1, Col3a1, Timp1*	Fibroblast	Mesenchyme	5817	114	648	5055
5	*Sftpd, Sftpc, Lcn2, Lamp3*	AT2	Epithelium	5266	34	935	4297
6	*Pdpn*	AT1	Epithelium	4849	31	518	4300
7	*Retnla, Cyp2f2, Scgb3a2*	Club1	Epithelium	3377	63	1077	2237
8	*Spp1*	Macrophage	Immunocyte	2994	453	764	1777
9	*Chil3*	Macrophage	Immunocyte	2723	184	350	2189
10	*Hpox, Inmt*	AT2	Epithelium	2575	2052	136	387
11	*Mmp12*	Macrophage	Immunocyte	2185	110	1213	862
12	*Hbb-bs, Hbb-a1, Hbb-a2, Hbb-bt*	Erythrocyte	RBC	2018	877	345	796
13	*Scgb3a1, Bpifa1, Bpifa2, Scgb3a2*	Club2	Epithelium	1993	707	189	1097
14	*Malat1*	AT1	Epithelium	1929	814	223	892
15	*Upk3b, Msln, Col3a1*	Mesothelial	Mesenchyme	1662	580	107	975
16	*Jchain, Igkc*	Plasma	Immunocyte	1658	221	279	1158
17	*Ighm*	B cell	Immunocyte	1604	134	416	1054
18	*Cyp2f2, Scgb3a2*	Club1	Epithelium	1553	1495	7	51
19	*Retnla, Cyp2f2, Scgb3a2, Trim71*	Club1	Epithelium	1536	NA	NA	1536
20	*Sftpb, Sftpd*	AT2	Epithelium	1529	12	214	1303
21	*S100a4*	Macrophage	Immunocyte	1279	244	338	697
22	*S100a8, S100a9, Ngp, Camp*	Neutrophil	Immunocyte	1114	381	188	545
23	*Myh6, Myl7*	Pulmonary vein myocardium	Mesenchyme	951	349	137	465
24	*Acta2, Actc1, Myl9, Myh11*	Smooth muscle	Mesenchyme	939	484	99	356
25	*Iglc1, Jchain*	Plasma	Immunocyte	333	49	44	240
26	*Abcb10*	Erythrocyte	RBC	311	98	40	173
27	*Ighm*	B cell	Immunocyte	79	79	NA	NA
Total				77687	21726	13439	42522

3.2. The atlas is consistent with known cell dynamics and gene expression profiles

We compared our spatiotemporal transcriptome data to the recently published single cell sequencing data of the bleomycin instillation model [15] (Fig. 2A and B). We found good consistency both between the epithelial single cells and the whole lung single cells, with major cell types identified in single cell data also presented in our spatial transcriptome data, even though we used different

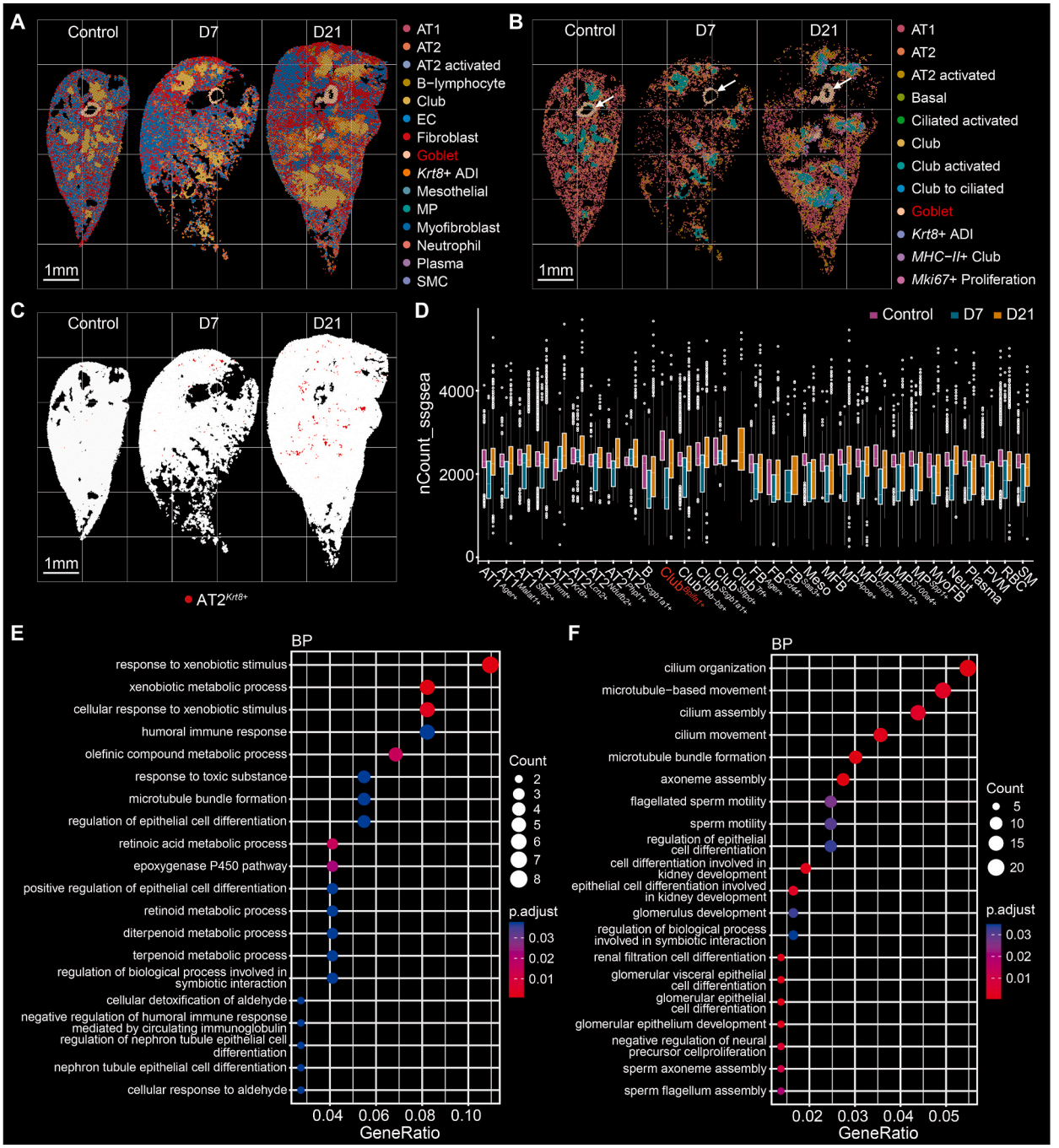

Fig. 2. Investigating known features during fibrosis in the spatiotemporal atlas. **A**, Mapping a published single-cell dataset of entire mouse lungs onto our spatiotemporal atlas. **B**, Mapping another published single-cell dataset of mouse lung epithelial cells onto our spatiotemporal atlas. **C**, Spatiotemporal distribution of AT2 cells expressing *Krt8* in our spatiotemporal atlas. **D**, Enrichment scores of genes known to have been associated with fibrosis in cell subtypes of our spatiotemporal atlas. **E**, GO enrichment analysis of the highly expressed genes in club$^{Bpifa1+}$. **F**, GO enrichment analysis of genes co-expressed with *MUC5B* in club$^{Bpifa1+}$.

marker genes, and the final cell type nominations were not the same. In this previous single cell sequencing study, a novel intermediate cell type differentiated from AT2 cells (expressing the gene *Krt8*), was found, and proved to be involved in AT1 cell regeneration and fibrogenesis. In our dataset, we also observed this cell type (Fig. 2C), and we found AT2^{Krt8+} in the lungs after bleomycin instillation but not in the control lung, which was also consistent with the previous findings. Overall, our dataset was comparable to the single cell sequencing data, but with spatial information available, it is unique for exploring in situ gene expression patterns and cell level dynamics.

With the spatiotemporal transcriptome dataset available, we then explored expression patterns of genes previously known to be related with fibrosis [3]. We calculated the enrichment scores of 33 known pulmonary fibrosis-related genes across all the cell subtypes, and interestingly, we found the enrichment scores of known genes in one subtype of club2 cells (club2$^{Bpifa1+}$) were significantly different during fibrosis (Fig. 2D). For example, *MUC5B* encodes a mucin protein, which would be the major contributor to the lubricating and viscoelastic properties of normal lung mucus. Previous genome-wide association study [16] identified the strongest risk polymorphism in promotor region of this gene, of which the risk allele would result in increased expression of *MUC5B* in terminal bronchi and honeycombed cysts of IPF affected lungs [32]. In our dataset, we observed increased gene expression of *MUC5B* in club2$^{Bpifa1+}$ cells in the 7d lung comparing to control lung, and its expression was downregulated in the 21d lung. This is consistent with the previous described regulatory mechanism of this gene in fibrosis. Furthermore, we checked the spatial distribution of these club2$^{Bpifa1+}$ cells to find them to be primarily distributed around the bronchial region and show quite high spatial specificity (Fig. 2B). The highly differentiated expression pattern of known fibrosis related genes during fibrosis in club2$^{Bpifa1+}$ cells reflected possible

Fig. 3. Cell dynamics after bleomycin instillation and during fibrosis. A, Pie chart to show the number and proportion of each cell type. **B**, Histogram to show the proportions of cell types after bleomycin instillation (control, 7d and 21d). **C**, Proportional changes, and spatiotemporal distribution of epithelial subtypes during fibrosis. **D**, Proportional changes and spatiotemporal distribution of fibroblast subtypes during fibrosis. **E**, Proportional changes and spatiotemporal distribution of Macrophage subtypes during fibrosis. **F**, Proportional changes, and spatiotemporal distribution of red blood cells during fibrosis. (For interpretation of the references to colour in this figure legend, the reader is referred to the Web version of this article.)

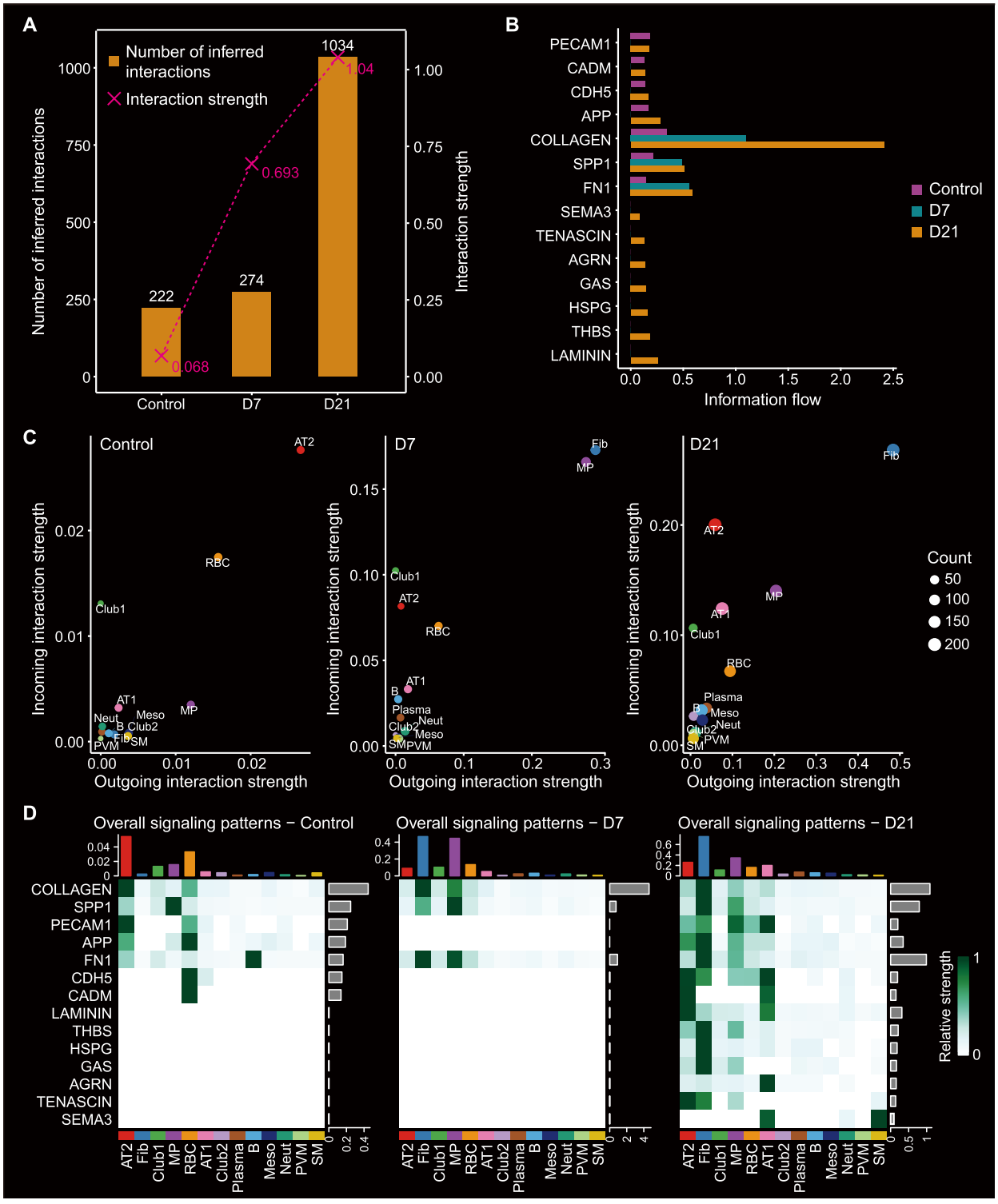

Fig. 4. Cell-cell interaction changes during fibrosis. **A**, Number, and strength of cell-cell interactions among all cells. **B**, Information flows fulfilled by different pathways during fibrosis. **C**, Input, and output signal strengths of cell types during fibrosis. **D**, Strength of various signaling pathways for cell types during fibrosis.

involvement of this cell type in pulmonary fibrosis. We finally explored the gene expression network within club2$^{Bpifa1+}$ cells to find possible fibrosis related genes. Differentially expressed genes with significantly higher expression compared to other cells and the genes co-expressed with *MUC5B* were found to be enriched in GO terms related to epithelial cell differentiation (Fig. 2E and F, Fig. S1A). For the known risk genes other than *MUC5B*, some also show cell type or even subtype specific expression and changed the expression along fibrosis, including *Abca3*, *Cdnk1a*, *Atp11a* and *Akap13*, while some were widely expressed in multiple cell types, including *Sftpc* and *Sftpa1*. *Sftpc* and *Sftpa1* showed differential gene expression during fibrosis across multiple cell types, reflecting complex roles they played during fibrosis (Fig. S1B). Taking together, using our dataset, we were able to elucidate the gene expression changes in different cell types or subtypes, which would aid exploring the molecular mechanisms of fibrosis.

3.3. The cell dynamics during fibrosis

The spatial transcriptome data represented large number of cells on sections, thus it provides the cell number and cell proportion information. Despite possible bias or differences resulted from section positions and angles, each section contains thousands of cells, therefore it could reflect overall cell proportions. We first summarized the total cell proportion based on the cell bins we obtained (Fig. 3A and B). We found AT2 cells, fibroblasts, club1 cells, MPs, RBCs and AT1 cells to be the major cell types, comprising more than 86 % of all cells. Among these major cell types, we found notable cell proportion changes during fibrosis, except club1 cells, which gradually reduced after bleomycin instillation. For AT2 cells, we found them to dramatically reduced after bleomycin instillation, contrasting to the obvious increase of AT1 cells and relatively subtle changes of club1 and club2 cells (Fig. 3C). Meanwhile, we found widely distributed AT2 cells were reduced and restrained to some areas during fibrosis (Fig. 3C), while AT1 cells were increased especially in lower lobe (Fig. 3C).

For fibroblasts, we found them to substantially increase (Fig. 3D) and fill the non-epithelial regions during the fibrosis (Fig. 3D). We then investigated the changes of fibroblast subtypes, to find increasing of originally existed fibroblast subtypes including FB^{Ager+}, FB^{Cd44+}, matrix fibroblast (MFB) and myofibroblasts (MyoFB). We noticed subtle reduction of FB^{Cd44+} and MFB in the 21d lung comparing to the 7d lung, indicating possible recover or progression of fibrosis in the 21d lung. MFBs are responsible for the synthesis and maintenance of the extracellular matrix (ECM) in tissues [33], thus their subtle decrease probably indicated fibrosis resolution. Meanwhile, MFBs can be differentiated into MyoFBs in response to mechanical stresses [34], and in our dataset we found MFBs to have probably triggered the increasing of MyoFB, which were steadily and substantially increased during the whole process. Finally, we found a fibroblast subtype, FB^{Saa3+}, to have been emerged and increased during fibrosis, of which the roles played during fibrosis awaits further investigations.

For macrophages, we found them to substantially increase in the 7d lung and then subtly decrease in the 21d lung, with almost all subtypes changed similarly (Fig. 3E). We also found the macrophages to increase in non-epithelial regions (Fig. 3E), like fibroblasts, indicating involvement of immune reactions in fibrosis. Lastly, we analyzed red blood cells (RBCs) in our dataset, which were usually not profiled in single cell sequencing studies. We observed a decrease in RBCs over time (Fig. 3F), which may be a result of fibrosis and could potentially exacerbate disease progression due to the ischemia and anoxia resulting from the reduction of RBCs. Overall, we comprehensively depicted the cell dynamics in the bleomycin induced mouse pulmonary fibrosis model, adding to our understanding of this IPF model.

3.4. Cell-cell interactions changed during fibrosis

In addition to the cell proportion changes we have observed, we investigated the cell-cell interactions among cell types/subtypes and the interaction changes during fibrosis (Table S1). In the control lung, the number of inferred cell-cell interactions were low, and the interaction strength was weak (Fig. 4A), among which AT2 cells and RBCs were found to have the strongest interactions with other cells (Fig. 4B and C). After bleomycin instillation, the 7d lung showed some increase in the number of inferred interactions and substantial increase of interaction strength. The signals related to cell adhesion, such as PECAM1, CADM, CDH5, and APP, show almost zero probability of interaction between cells, which indicates the existence of cell migration in the 7d lung (Fig. 4B). With the number of AT2 cells decreasing, their role in affecting other cells reflected by outgoing interaction strength was weakened, while the interaction strength of fibroblasts and macrophages with other cells was greatly improved (Fig. 4C). Further looking at the signaling patterns, we found COLLGEN to be the major molecule effective in these cell-cell interactions (Fig. 4D), which is related to extracellular matrix deposition. This reflected that with the increase of fibroblasts and macrophages, they were affecting other cells through proteins including COLLGEN, SPP1, FN1, etc., to result in fibrosis. In the 21d lung, we found the cell-cell interactions to be the strongest with large number of interactions (Fig. 4A), and the cell interactions of all cell types were improved with the proteins of CDH5, LAMININ, THBS, HSPG, GAS, AGRN, SEMA3, etc. (Fig. 4D) as the communication molecular, which are related to vascular development and vascular homeostasis [35,36]. Among all cell types, fibroblasts, macrophages and AT1 cells were improved most in cell-cell interactions, while club1 cells were least changed. Considering persistent fibrosis process and initiation of possible self-resolving in the 21d lung, the detailed cell-cell interaction dynamics illustrated here provided valuable information for understanding the relationship among cell types and inferring possible intervention targets.

3.5. Epithelial cell differentiation during fibrosis

Epithelial cells played critical roles in normal lung function and in lung pathogenesis including fibrosis [37]. In normal lungs, epithelial cells provide surface areas, thus serve as mediators of gas exchange, with AT2 cells to produce surfactant and replace injured

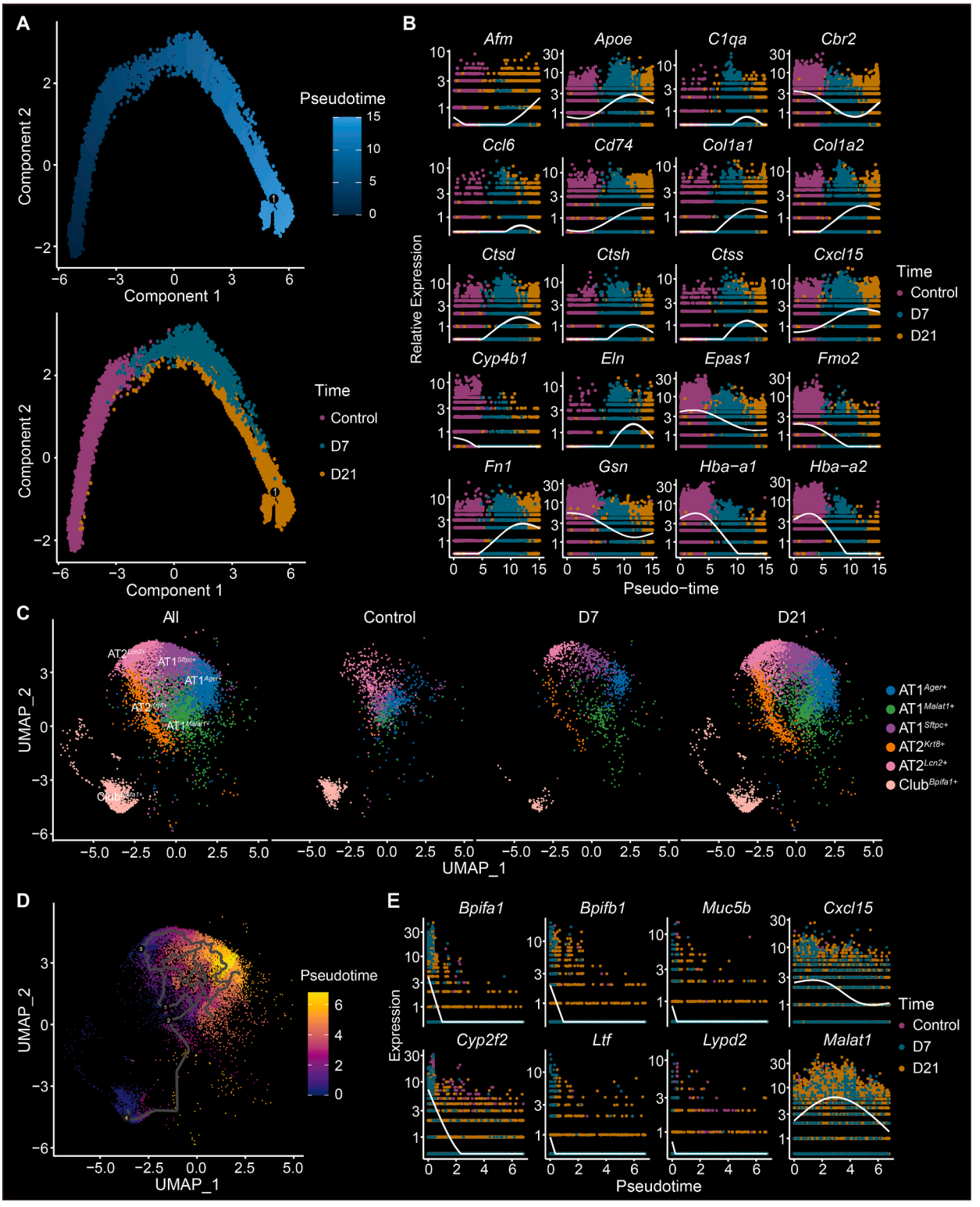

Fig. 5. Epithelial cell differentiation during fibrosis. A, Differentiation trajectory of AT2 cells. **B**, Genes related to AT2 cell differentiation. **C**, UMAP of epithelial cell subtypes related to differentiation during fibrosis. **D**, UMAP and pseudotime of epithelial cells related to differentiation.

AT1 cells through cell differentiation [38]. In lung diseases like IPF, abnormal epithelial cell differentiation was usually observed, with the inability of AT2 cells to repair injured AT1 cells or AT2 cells to differentiate to other cell types [5,39]. Thus, we investigated the epithelial cell differentiation in our dataset. We first analyzed the differentiation of AT2 cells (Fig. 5A) to find a gradually evolving/developing process of AT2 cells after bleomycin instillation. AT2 cells in the 7d lung were different from those in the control lung and were further developed to AT2 cells in the 21d lung, which were the most mature/developed AT2 cells. Along this pseudotime cell differentiation, we identified critical genes including well known fibrosis related genes like *Col1a1*, *Col1a2*, *Eln* and *Fn1* (Fig. 5B, Table S2). We also find *Epas1*, which is a transcription factor previously reported to be involved in promoting hypoxic pulmonary hypertension [40], to change in accordance with the AT2 differentiation, indicating involvement of oxygen related pathway in fibrosis. We found expressions of these genes to first increase in the 7d lung and then decrease to some extent in the 21d lung (*Epas1* was in the opposite trend), again indicating possible resolution from fibrosis. To further support that, we found AT2 cells in the 21d lung to occupy the whole AT2 cell pseudotime differentiation path, with cells similar to both the AT2 cells in the control lung and those in the 7d lung (Fig. 5A). Overall, AT2 cells were found to differentiate during fibrosis and AT2 cells in the 21d lung seemed to slightly recover original AT2 cell functions.

Since AT1 cells were increased during fibrosis and previous studies already suggested AT2 to AT1 differentiation [41], we then investigated the differentiation from other epithelial cells to AT1 cells (Fig. 5C). We confirmed the differentiation path of AT2 cells to AT1 cells in the 7d lung and the 21d lung (Fig. 5D). We also confirmed the existence of the activated AT2 cells ($AT2^{Lcn+}$) and the previously reported AT2 subtype, $AT2^{Krt8+}$. Meanwhile, we found the differentiation path from a subtype of club cells, $club^{Bpfa1+}$ to be able to differentiate to $AT2^{Krt8+}$ (Fig. 5D, Figs. S2A and S2B). However, our pseudotime analysis results indicated $AT2^{Krt8+}$ cells to be more likely a final status instead of an intermediate cell type (Figs. S2C and S2D). We think the differentiation to $AT2^{Krt8+}$ cells during fibrosis might have large effects on the fibrosis procedure, which awaits further exploration. We finally explored genes that drive epithelial cell differentiation, to identify genes including *Bpifa1*, *Muc5b*, *Cyp2f2*, *Ltf*, etc (Fig. 5E, Table S3). *Bpifa1* is a critical component of the innate immune response that prevents upper airway diseases [42]. Cytochromes P450 (CYPs) are a multigene superfamily of constitutively expressed and inducible enzymes responsible for the detoxification of many endogenous and exogenous

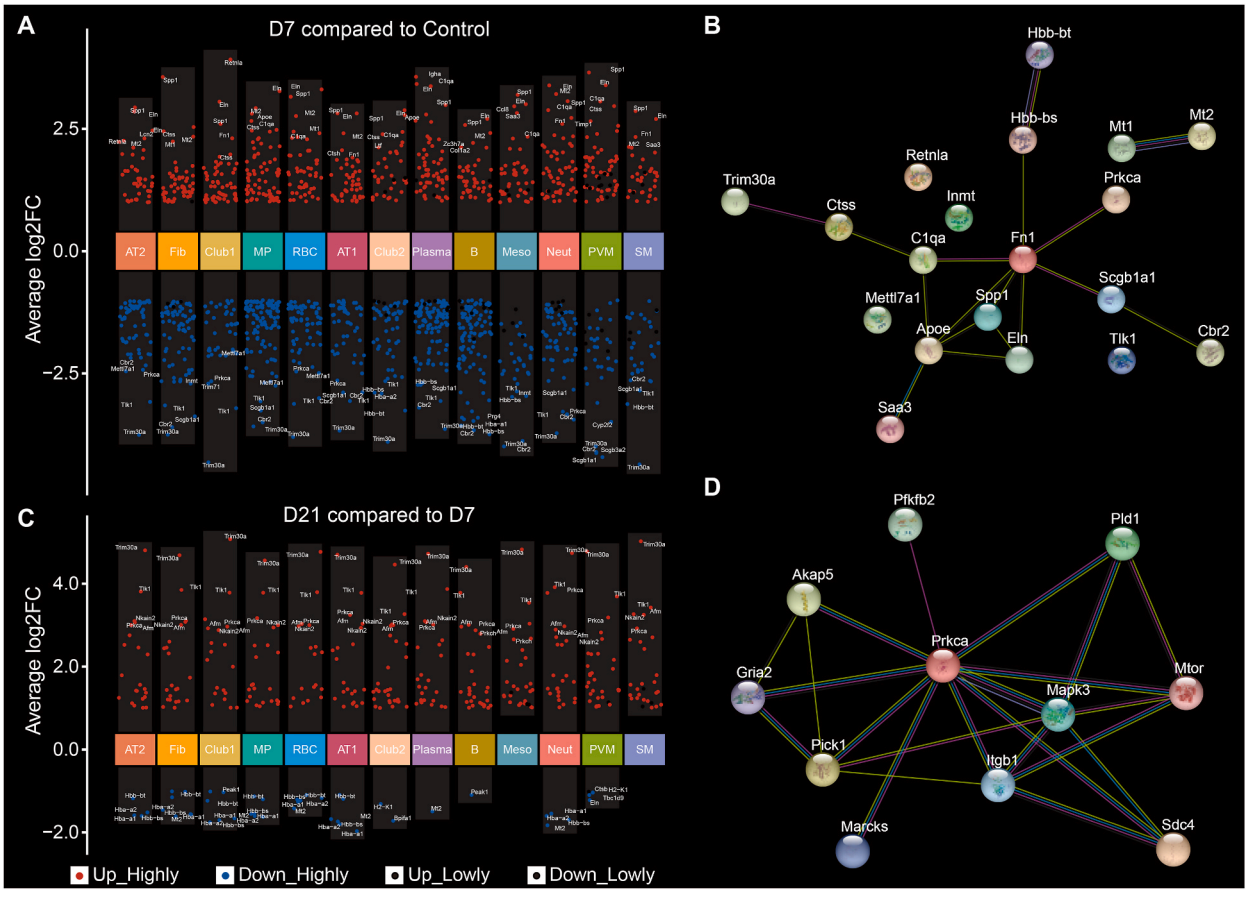

Fig. 6. Possible genes related to fibrosis and self-resolving. A, Significantly differentially expressed genes in different cell types comparing the 7d lung days to the control lung. **B**, Differentially Expressed Gene Protein Interaction Network comparing the 7d lung days to the control lung. **C**, Significantly differentially expressed genes in different cell types comparing the 21d lung to the 7d lung. **D**, Network of genes which can interact with Prkca protein.

compounds and for the metabolism of numerous medications [43]. *LTF* is a protective gene in PRAD, and its downregulation will inhibit the normal immune response in the body [44]. By utilizing these genes to induce epithelial cell differentiation, we hypothesize that this process may play a protective role in fibrosis, thereby offering additional insights into the molecular-level alterations associated with epithelial differentiation in pulmonary fibrosis.

3.6. Genes related to fibrosis and self-resolving

In addition to cell dynamics along fibrosis, we further analyzed the gene expression changes to reveal important genes related with fibrosis and self-resolving. We compared the 7d lung to the control lung in the gene expression across all the thirteen cell types (Fig. 6A), and we extracted genes to show expression changes across majority of cell types. Within these genes of which the expression vastly changed, we found genes including *Spp1*, *Eln*, *Fn1*, *Mt2* (upregulated), and *Trim30a*, *Scgb1a1*, *Cbr2*, *Tlk1*, *Prkca*, *Mettl7a1* (downregulated) (Table S4). Clustering these genes resulted in one major gene cluster with *Fn1*, *Spp1*, *Eln*, *Apoe* and other genes as hub genes (Fig. 6B), and functional enrichment of these genes reflected enriched functions in cell migration, extracellular structures (related to fibrosis) and damage repair (Fig. S3A). Among these upregulated genes, *Spp1* was previously found to be expressed in macrophages, which would activate the myofibroblasts in IPF [45], and its expression was increased during mouse lung fibrosis [46]. *Eln* encodes components of elastin which can stimulate the migration and proliferation of monocytes and fibroblasts, and previous study found it to be upregulated in chronic obstructive pulmonary disease (COPD) affected lungs [47]. Within the downregulated genes, *Cbr2* encodes carbonyl reductase, which was involved in arachidonic acid pathway and related with anti-apoptosis and anti-inflammation [48]. *Trim30a* encodes a *trans*-acting factor, which was proved to function in protect from endotoxin shock in mouse [49]. *Prkca* encodes a protein kinase C, which was found to be involved in alleviating acute lung injury and inflammatory response [50]. Downregulation of these gene with protective roles might have aggravated the injury of bleomycin and promoted the fibrosis procedure.

Comparing the 21d lung to the control lung (Fig. S3B, Table S5), other than the genes overlapped with the above comparison (the 7d lung to the control lung), we also found fibrosis related genes to have been commonly upregulated, including genes like *Col1a1* and *Col1a2*, which were suggested as potential biomarkers for pulmonary fibrosis [51]. Meanwhile, the difference was obvious in the downregulated genes. In the 21d lung to the control lung comparison, we found the commonly downregulated genes to be hemoglobin related genes, which might be a result of fibrosis to affect the major lung function of blood oxygen exchange.

We then compared the gene expression changes in the 21d lung and the 7d lung (Fig. 6C, Table S6), to reveal the expression dynamics in later stage of fibrosis. We carried out enrichment analysis for the differentially expressed genes shared among different cell types to reflect the changes in this stage. First, we can still find some signals of fibrosis with the genes involved in cell migrations to be enriched (Fig. S3C), although the enriched terms were different from the previous comparisons (the 7d lung to the control lung). But we found genes involved in wound healing, apoptotic signaling pathway to be enriched, including oxidative phosphorylation and response to oxidative stress, which once more, reflected possible self-resolving of fibrosis. Further looking at all differentially expressed genes across cell lines in the 7d lung to the control lung comparison and the 21d lung to 7d lung comparison (Fig. S3), we found 132 genes to have functions related with injury repair, of which 38 were showing significant expression changes (Fig. S4, Table S7). These genes should be probable self-resolving related genes. Especially in the 21d lung to the 7d lung comparison, we identified commonly upregulated genes to have possible regulation functions and to be involved in damage repair (Fig. S3C), including *Tlk1*, *Trim30a*, *Afm*, *Nkain2* and *Prkca* to be commonly upregulated. *Afm* encodes a possible hydrophobic molecule carrier protein and *Nkain2* encodes a transmembrane protein, which we did not know their possible functions during fibrosis. *Tlk1* encodes a serine/threonine kinase, which were found to be function in anti-apoptosis [52,53]. *Trim30a* was found in the 7d lung to the control lung comparison to be downregulated (as described above), and it should have the function of regulating endotoxin shock [49]. *Prkca*, which was also found in the 7d lung to the control lung comparison to be downregulated, was reported to be involved in alleviation of acute lung injury [50]. We further investigated the proteins interacting with the protein kinase C encoded by *Prkca* (Fig. 6D), to find genes like *Marcks* (encoding myristoylated alanine rich protein kinase C substrate) and *Mapk3* (encoding mitogen-activated protein kinase), which are associated with mitosis [54,55]. We found these two genes to have been significantly upregulated in the 21d lung (Fig. S5). Furthermore, we investigated the *Prkca* involved KEGG pathways to find the downstream genes (Fig. S5), including *Vegfd* (encoding vascular endothelial growth factor) and *Mmp2* (encoding matrix metallopeptidase 2 which might aid degradation of ECM [56]). These two genes were also upregulated, with the expression recovery of *Prkca*. Taking together, we found genes, including *Prkca*, to be possibly related with the self-resolving of fibrosis in the bleomycin induced lung fibrosis mouse model, which awaits further investigations.

4. Discussion

Pulmonary fibrosis is a common phenotype of multiple pulmonary diseases, lacking effective intervention or treatment methods. Research, developing of drugs, as well as developing of clinical interventions require an effective disease model. Therefore, we studied the commonly used mouse model of pulmonary fibrosis induced by a single dose of bleomycin instillation using the cutting-edge spatial transcriptome technique, Stereo-seq. We constructed a spatiotemporal transcriptome atlas of mouse pulmonary fibrosis by in-situ spatial sequencing of mouse lungs at three time points including before injection, 7 days after injection, and 21 days after injection. Through the analysis of the atlas, we first comprehensively annotated the various cell types, to find clear signals of fibrosis in the lungs after bleomycin injection. We found substantial changes in epithelial cells, fibroblasts, macrophages, and red blood cells during fibrosis. In epithelial cells, a sharp decrease in AT2 cells was accompanied by a significant increase in AT1 cells. Fibroblasts increased overall, but there were different trends in subtypes after 7 days. The changes observed in various subtypes of macrophages exhibited a

similar pattern, with all subtypes increasing in the 7d lung and decreasing in the 21d lung. We were also able to analyze the RBCs to find them consistently and substantially reduced throughout fibrosis. The changes in cell types also correlated with the interactions between cells. During fibrosis, the interactions between fibroblasts and macrophages and other cell types are increased. In contrast, AT2 cells and RBCs were the major cell types interacting with other cell types in normal lung. We further analyzed the differentiation of epithelial cells. In the process of fibrosis, we confirmed that AT2 cells can differentiate into a subtype of $AT2^{Krt8+}$ reported before [15]. We also found that the club cells subtype we annotated ($club^{Bpfa1+}$) can also differentiate to $AT2^{Krt8+}$ cells, and we analyzed to find $AT2^{Krt8+}$ to be more likely a terminal cell type rather than an intermediate cell type. Finally, we also analyzed the gene expression changed to find *Prcka* and other potential self-resolving related genes. Our study on mouse fibrosis models using Stereo-seq largely replicated the results of previous single-cell sequencing study [15]. Spatial transcriptome data provided in-situ gene expression profiling of more cells comparing to single-cell sequencing. All the cells within a section of the mouse lungs were profiled and then used for identifying cell types and analyzing cellular changes, with tens to hundreds and thousands of cells. Secondly, spatial transcriptomes provide the spatial position information of cells, thus direct investigations of changed cell types or novel cell types, as well as their relationship with other cells, were feasible. For example, we found that fibroblasts and macrophages both increased in the non-epidermal regions, reflecting the possible joint changes. Of course, the current spatial transcriptome technology also has limitations, such as the absence of cell boundary information and to use cell bins to represent might introduce some bias. We used the previous single cell sequencing data to indicate the efficiency and accuracy of our cell bin analysis.

In this study, we injected single dose bleomycin (1.8 U/kg) to induce the pulmonary fibrosis, which was lower comparing to the previous study (3 U/kg) [15]. Although the lower dosage we used also induced fibrosis indicating by corresponding fibrosis markers, we think lower dosage might have resulted in faster self-resolving, reflected through several aspects. We found the overall fibroblasts to increase, and especially the subtype of myofibroblasts increased steadily. Since myofibroblasts majorly contributed to abnormal accumulation of ECM, this reflected ongoing fibrosis in the 21d lung. But we observed cellular level recovery including subtle increase of AT2 cells and club2 cells, decrease of macrophages, B cells, as well as backwards changes of subtypes of fibroblasts, comparing the 21d lung to the 7d lung. Moreover, comparing the gene expression of the 7d lung to the control lung, we were able to find genes involved in fibrosis to be upregulated prevalently while comparing 21d lung to the control lung, we only identified hemoglobin related genes to be prevalently upregulated and fibrosis related genes to be downregulated. Thus, we compared the 21d lung to the 7d lung in gene expression to identify the upregulated genes, of which the function annotations indicated them as non-fibrosis related genes. Investigating previous publications on these genes, we proved them as possible self-resolving related genes as they were reported to function in cell regulations. Although we did not carry out in depth validations, expression patterns of these genes in previous datasets supported them as effective for mouse pulmonary fibrosis and they were probably not invoked in human pulmonary fibrosis. Future studies on these genes would accelerate our understanding of the self-resolving in the bleomycin induced pulmonary fibrosis model and shed lights on the possible targets to intervening the fibrosis process. Despite the findings in our study, we need to admit that the samples were limited, and biological replications were lacking. Although we were able to use the previous single cell sequencing data to prove our data quality, it would be more informative if there can be more samples from more time points after the bleomycin instillation.

5. Limitations of this study

Our study aimed to investigate the molecular changes associated with bleomycin-induced pulmonary fibrosis using mouse models and spatial transcriptomics technology. While our findings provide valuable insights into this disease, there are several limitations that should be considered. One limitation of our study is that we used a limited number of mouse models. While mouse models are widely used to study pulmonary fibrosis, the extent to which they represent the disease is not fully understood, particularly considering the uncertainty of different doses of bleomycin. Therefore, our results should be interpreted with caution, and further studies using a larger number of mouse models, as well as other animal models and human samples, are needed to validate our findings. Another limitation of our study is that we identified key gene expression changes at the cellular and molecular levels, but we did not investigate the functional consequences of these changes. Further studies are needed to investigate the functional significance of these molecular changes and their potential role in the development and progression of pulmonary fibrosis. Despite these limitations, our study provides a foundation for further research into the molecular mechanisms of pulmonary fibrosis and may aid in the development of new therapeutic strategies for the disease by identifying potential targets for treatment. By elucidating the key gene expression changes and molecular processes involved in lung fibrosis, our study may help to identify novel pathways and molecules that could be targeted to prevent or treat this devastating disease.

Ethics approval statement

All relevant procedures involving animal experiments presented in this paper were approved by Animal Care and Use Committee of Tongji Hospital, Tongji Medical College, Huazhong University of Sciences and Technology (TJH-202109025).

Data availability statement

All raw data generated by Stereo-seq have been deposited to CNGB Spatial Transcript Omics DataBase: STT0000032 (https://db.cngb.org/stomics/).

The mouse single-cell RNA sequencing (scRNA-seq) data can be accessed through the Gene Expression Omnibus (GEO) database

using the accession code GSE141259, while the human scRNA-seq data are available with the accession code GSE135893.

CRediT authorship contribution statement

Qingsong Li: Visualization, Software, Methodology, Investigation, Formal analysis. **Yue Wang:** Visualization, Software, Methodology, Investigation, Formal analysis. **Liu Ji:** Methodology, Investigation, Formal analysis. **Jianhan He:** Methodology, Investigation, Formal analysis. **Haixia Liu:** Methodology, Data curation. **Weizhen Xue:** Methodology, Data curation. **Huihui Yue:** Methodology, Data curation. **Ruihan Dong:** Software, Methodology. **Xin Liu:** Writing – review & editing, Writing – original draft, Supervision, Funding acquisition, Conceptualization. **Daqing Wang:** Writing – original draft, Supervision, Conceptualization. **Huilan Zhang:** Writing – review & editing, Supervision, Resources, Project administration, Conceptualization.

Declaration of competing interest

The authors declare that they have no known competing financial interests or personal relationships that could have appeared to influence the work reported in this paper.

Acknowledgments

This study was supported by the National Natural Science Foundation of China (81974456 and 82170081) and the Ministry of Science and Technology of the People's Republic of China (2021YFC2500701). We are also grateful for the commitment of the China National GeneBank (CNGB) in advancing genomics, biotechnology, and translational medicine, as well as for their efforts in establishing a national platform for the protection, sharing, and application of genetic resources.

Appendix T. Supplementary data

Supplementary data to this article can be found online at https://doi.org/10.1016/j.heliyon.2023.e22461.

Abbreviations

AT1	alveolar type I
AT2	alveolar type II
ECM	extracellular matrix
FB	fibroblast
IPF	Idiopathic pulmonary fibrosis
Meso	mesothelial cells
MFB	matrix fibroblast
MP	macrophages
MyoFB	myofibroblasts
Neut	neutrophil
PVM	pulmonary vein myocardium
RBC	red blood cells
SM	smooth muscle
Stereo-seq	SpaTial Enhanced REsolution Omics-sequencing

References

[1] G. Raghu, Epidemiology, survival, incidence and prevalence of idiopathic pulmonary fibrosis in the USA and Canada, Eur. Respir. J. 49 (2017), https://doi.org/10.1183/13993003.02384-2016.

[2] F.J. Martinez, H.R. Collard, A. Pardo, G. Raghu, L. Richeldi, M. Selman, J.J. Swigris, H. Taniguchi, A.U. Wells, Idiopathic pulmonary fibrosis, Nat Rev Dis Primers 3 (2017), 17074, https://doi.org/10.1038/nrdp.2017.74.

[3] B.J. Moss, S.W. Ryter, I.O. Rosas, Pathogenic mechanisms underlying idiopathic pulmonary fibrosis, Annu. Rev. Pathol. 17 (2022) 515–546, https://doi.org/10.1146/annurev-pathol-042320-030240.

[4] P.A. Reyfman, J.M. Walter, N. Joshi, K.R. Anekalla, A.C. McQuattie-Pimentel, S. Chiu, R. Fernandez, M. Akbarpour, C.I. Chen, Z. Ren, et al., Single-cell transcriptomic analysis of human lung provides insights into the pathobiology of pulmonary fibrosis, Am. J. Respir. Crit. Care Med. 199 (2019) 1517–1536, https://doi.org/10.1164/rccm.201712-2410OC.

[5] T.S. Adams, J.C. Schupp, S. Poli, E.A. Ayaub, N. Neumark, F. Ahangari, S.G. Chu, B.A. Raby, G. DeIuliis, M. Januszyk, et al., Single-cell RNA-seq reveals ectopic and aberrant lung-resident cell populations in idiopathic pulmonary fibrosis, Sci. Adv. 6 (2020), eaba1983, https://doi.org/10.1126/sciadv.aba1983.

[6] A.C. Habermann, A.J. Gutierrez, L.T. Bui, S.L. Yahn, N.I. Winters, C.L. Calvi, L. Peter, M.I. Chung, C.J. Taylor, C. Jetter, et al., Single-cell RNA sequencing reveals profibrotic roles of distinct epithelial and mesenchymal lineages in pulmonary fibrosis, Sci. Adv. 6 (2020), eaba1972, https://doi.org/10.1126/sciadv.aba1972.

[7] D.M. Walters, S.R. Kleeberger, Mouse models of bleomycin-induced pulmonary fibrosis. Curr Protoc Pharmacol *Chapter*, Unit 5 46. 10.1002/0471141755.ph0546s40 5 (2008).

[8] K. Komura, K. Yanaba, M. Horikawa, F. Ogawa, M. Fujimoto, T.F. Tedder, S. Sato, CD19 regulates the development of bleomycin-induced pulmonary fibrosis in a mouse model, Arthritis Rheum. 58 (2008) 3574–3584, https://doi.org/10.1002/art.23995.

[9] K. Aoshiba, T. Tsuji, S. Kameyama, M. Itoh, S. Semba, K. Yamaguchi, H. Nakamura, Senescence-associated secretory phenotype in a mouse model of bleomycin-induced lung injury, Exp. Toxicol. Pathol. 65 (2013) 1053–1062, https://doi.org/10.1016/j.etp.2013.04.001.

[10] Y. Wang, S. Hu, L. Shen, S. Liu, L. Wan, S. Yang, M. Hou, X. Tian, H. Zhang, K.F. Xu, Dynamic observation of autophagy and transcriptome profiles in a mouse model of bleomycin-induced pulmonary fibrosis, Front. Mol. Biosci. 8 (2021), 664913, https://doi.org/10.3389/fmolb.2021.664913.

[11] H.J. Park, O.Y. Jeong, S.H. Chun, Y.H. Cheon, M. Kim, S. Kim, S.I. Lee, Butyrate improves skin/lung fibrosis and intestinal dysbiosis in bleomycin-induced mouse models, Int. J. Mol. Sci. 22 (2021), https://doi.org/10.3390/ijms22052765.

[12] R. Zhang, W. Jing, C. Chen, S. Zhang, M. Abdalla, P. Sun, G. Wang, W. You, Z. Yang, J. Zhang, et al., Inhaled mRNA nanoformulation with biogenic ribosomal protein reverses established pulmonary fibrosis in a bleomycin-induced murine model, Adv Mater 34 (2022), e2107506, https://doi.org/10.1002/adma.202107506.

[13] I.G. Luzina, E.P. Lillehoj, V. Lockatell, S.W. Hyun, K.N. Lugkey, A. Imamura, H. Ishida, C.W. Cairo, S.P. Atamas, S.E. Goldblum, Therapeutic effect of neuraminidase-1-selective inhibition in mouse models of bleomycin-induced pulmonary inflammation and fibrosis, J Pharmacol Exp Ther 376 (2021) 136–146, https://doi.org/10.1124/jpet.120.000223.

[14] S. Song, Z. Fu, R. Guan, J. Zhao, P. Yang, Y. Li, H. Yin, Y. Lai, G. Gong, S. Zhao, et al., Intracellular hydroxyproline imprinting following resolution of bleomycin-induced pulmonary fibrosis, Eur. Respir. J. 59 (2022), https://doi.org/10.1183/13993003.00864-2021.

[15] M. Strunz, L.M. Simon, M. Ansari, J.J. Kathiriya, I. Angelidis, C.H. Mayr, G. Tsidiridis, M. Lange, L.F. Mattner, M. Yee, et al., Alveolar regeneration through a Krt8+ transitional stem cell state that persists in human lung fibrosis, Nat. Commun. 11 (2020) 3559, https://doi.org/10.1038/s41467-020-17358-3.

[16] M.A. Seibold, A.L. Wise, M.C. Speer, M.P. Steele, K.K. Brown, J.E. Loyd, T.E. Fingerlin, W. Zhang, G. Gudmundsson, S.D. Groshong, et al., A common MUC5B promoter polymorphism and pulmonary fibrosis, N. Engl. J. Med. 364 (2011) 1503–1512, https://doi.org/10.1056/NEJMoa1013660.

[17] T.E. Fingerlin, E. Murphy, W. Zhang, A.L. Peljto, K.K. Brown, M.P. Steele, J.E. Loyd, G.P. Cosgrove, D. Lynch, S. Groshong, et al., Genome-wide association study identifies multiple susceptibility loci for pulmonary fibrosis, Nat. Genet. 45 (2013) 613–620, https://doi.org/10.1038/ng.2609.

[18] A.Q. Thomas, K. Lane, J. Phillips 3rd, M. Prince, C. Markin, M. Speer, D.A. Schwartz, R. Gaddipati, A. Marney, J. Johnson, et al., Heterozygosity for a surfactant protein C gene mutation associated with usual interstitial pneumonitis and cellular nonspecific interstitial pneumonitis in one kindred, Am. J. Respir. Crit. Care Med. 165 (2002) 1322–1328, https://doi.org/10.1164/rccm.200112-123OC.

[19] R.J. Allen, B. Guillen-Guio, J.M. Oldham, S.F. Ma, A. Dressen, M.L. Paynton, L.M. Kraven, M. Obeidat, X. Li, M. Ng, et al., Genome-wide association study of susceptibility to idiopathic pulmonary fibrosis, Am. J. Respir. Crit. Care Med. 201 (2020) 564–574, https://doi.org/10.1164/rccm.201905-1017OC.

[20] J.M. Oldham, S.-F. Ma, F.J. Martinez, K.J. Anstrom, G. Raghu, D.A. Schwartz, E. Valenzi, L. Witt, C. Lee, R. Vij, et al., TOLLIP, MUC5B, and the response to N-acetylcysteine among individuals with idiopathic pulmonary fibrosis, Am. J. Respir. Crit. Care Med. 192 (2015) 1475–1482, https://doi.org/10.1164/rccm.201505-1010OC.

[21] A. Chen, S. Liao, M. Cheng, K. Ma, L. Wu, Y. Lai, X. Qiu, J. Yang, J. Xu, S. Hao, et al., Spatiotemporal transcriptomic atlas of mouse organogenesis using DNA nanoball-patterned arrays, Cell 185 (2022) 1777, https://doi.org/10.1016/j.cell.2022.04.003, 1792 e1721.

[22] C. Liu, R. Li, Y. Li, X. Lin, K. Zhao, Q. Liu, S. Wang, X. Yang, X. Shi, Y. Ma, et al., Spatiotemporal mapping of gene expression landscapes and developmental trajectories during zebrafish embryogenesis, Dev. Cell 57 (2022) 1284, https://doi.org/10.1016/j.devcel.2022.04.009, 1298 e1285.

[23] Z. Ou, S. Lin, J. Qiu, W. Ding, P. Ren, D. Chen, J. Wang, Y. Tong, D. Wu, A. Chen, et al., Single-nucleus RNA sequencing and spatial transcriptomics reveal the immunological microenvironment of cervical squamous cell carcinoma, Adv. Sci. 9 (2022), e2203040, https://doi.org/10.1002/advs.202203040.

[24] X. Wei, S. Fu, H. Li, Y. Liu, S. Wang, W. Feng, Y. Yang, X. Liu, Y.Y. Zeng, M. Cheng, et al., Single-cell Stereo-seq reveals induced progenitor cells involved in axolotl brain regeneration, Science 377 (2022), eabp9444, https://doi.org/10.1126/science.abp9444.

[25] Y. Hao, S. Hao, E. Andersen-Nissen, W.M. Mauck 3rd, S. Zheng, A. Butler, M.J. Lee, A.J. Wilk, C. Darby, M. Zager, et al., Integrated analysis of multimodal single-cell data, Cell 184 (2021) 3573, https://doi.org/10.1016/j.cell.2021.04.048, 3587 e3529.

[26] S. Jin, C.F. Guerrero-Juarez, L. Zhang, I. Chang, R. Ramos, C.H. Kuan, P. Myung, M.V. Plikus, Q. Nie, Inference and analysis of cell-cell communication using CellChat, Nat. Commun. 12 (2021) 1088, https://doi.org/10.1038/s41467-021-21246-9.

[27] C. Trapnell, D. Cacchiarelli, J. Grimsby, P. Pokharel, S. Li, M. Morse, N.J. Lennon, K.J. Livak, T.S. Mikkelsen, J.L. Rinn, The dynamics and regulators of cell fate decisions are revealed by pseudotemporal ordering of single cells, Nat. Biotechnol. 32 (2014) 381–386, https://doi.org/10.1038/nbt.2859.

[28] X. Qiu, Q. Mao, Y. Tang, L. Wang, R. Chawla, H.A. Pliner, C. Trapnell, Reversed graph embedding resolves complex single-cell trajectories, Nat. Methods 14 (2017) 979–982, https://doi.org/10.1038/nmeth.4402.

[29] T. Wu, E. Hu, S. Xu, M. Chen, P. Guo, Z. Dai, T. Feng, L. Zhou, W. Tang, L. Zhan, et al., clusterProfiler 4.0: a universal enrichment tool for interpreting omics data, Innovation 2 (2021), 100141, https://doi.org/10.1016/j.xinn.2021.100141.

[30] M. C, org.Mm.eg.db, in: Genome Wide Annotation for Mouse, 2022. R package version 3.15.0.

[31] N.M. Negretti, E.J. Plosa, J.T. Benjamin, B.A. Schuler, A.C. Habermann, C.S. Jetter, P. Gulleman, C. Bunn, A.N. Hackett, M. Ransom, et al., A single-cell atlas of mouse lung development, Development 148 (2021), https://doi.org/10.1242/dev.199512.

[32] I.V. Yang, T.E. Fingerlin, C.M. Evans, M.I. Schwarz, D.A. Schwartz, MUC5B and idiopathic pulmonary fibrosis, Ann Am Thorac Soc 12 (Suppl 2) (2015) S193–S199, https://doi.org/10.1513/AnnalsATS.201503-110AW.

[33] C. Vasquez, N. Benamer, G.E. Morley, The cardiac fibroblast: functional and electrophysiological considerations in healthy and diseased hearts, J. Cardiovasc. Pharmacol. 57 (2011) 380–388, https://doi.org/10.1097/FJC.0b013e31820cda19.

[34] I.A. Darby, B. Laverdet, F. Bonte, A. Desmouliere, Fibroblasts and myofibroblasts in wound healing, Clin Cosmet Investig Dermatol 7 (2014) 301–311, https://doi.org/10.2147/CCID.S50046.

[35] L. Montalva, L. Antounians, A. Zani, Pulmonary hypertension secondary to congenital diaphragmatic hernia: factors and pathways involved in pulmonary vascular remodeling, Pediatr. Res. 85 (2019) 754–768, https://doi.org/10.1038/s41390-019-0345-4.

[36] L.F. Yousif, J. Di Russo, L. Sorokin, Laminin isoforms in endothelial and perivascular basement membranes, Cell Adh Migr 7 (2013) 101–110, https://doi.org/10.4161/cam.22680.

[37] C.E. Barkauskas, M.J. Cronce, C.R. Rackley, E.J. Bowie, D.R. Keene, B.R. Stripp, S.H. Randell, P.W. Noble, B.L. Hogan, Type 2 alveolar cells are stem cells in adult lung, J. Clin. Invest. 123 (2013) 3025–3036, https://doi.org/10.1172/JCI68782.

[38] A.M. Olajuyin, X. Zhang, H.L. Ji, Alveolar type 2 progenitor cells for lung injury repair, Cell Death Discov 5 (2019) 63, https://doi.org/10.1038/s41420-019-0147-9.

[39] M. Chilosi, V. Poletti, B. Murer, M. Lestani, A. Cancellieri, L. Montagna, P. Piccoli, G. Cangi, G. Semenzato, C. Doglioni, Abnormal re-epithelialization and lung remodeling in idiopathic pulmonary fibrosis: the role of deltaN-p63, Lab. Invest. 82 (2002) 1335–1345, https://doi.org/10.1097/01.lab.0000032380.82232.67.

[40] S. Wang, Y. Wang, C. Liu, G. Xu, W. Gao, J. Hao, M. Zhang, G. Wu, Y. Yang, J. Huang, et al., EPAS1 (endothelial PAS domain protein 1) orchestrates transactivation of endothelial ICAM1 (intercellular adhesion molecule 1) by small nucleolar RNA host gene 5 (SNHG5) to promote hypoxic pulmonary hypertension, Hypertension 78 (2021) 1080–1091, https://doi.org/10.1161/HYPERTENSIONAHA.121.16949.

[41] J. Choi, J.E. Park, G. Tsagkogeorga, M. Yanagita, B.K. Koo, N. Han, J.H. Lee, Inflammatory signals induce AT2 cell-derived damage-associated transient progenitors that mediate alveolar regeneration, Cell Stem Cell 27 (2020) 366–382.e367, https://doi.org/10.1016/j.stem.2020.06.020.

[42] Y.A. Tsou, M.C. Tung, K.A. Alexander, W.D. Chang, M.H. Tsai, H.L. Chen, C.M. Chen, The role of BPIFA1 in upper airway microbial infections and correlated diseases, BioMed Res. Int. 2018 (2018), 2021890, https://doi.org/10.1155/2018/2021890.

[43] T.T.H. Dang, M. Choi, H.G. Pham, J.W. Yun, Cytochrome P450 2F2 (CYP2F2) negatively regulates browning in 3T3-L1 white adipocytes, Eur. J. Pharmacol. 908 (2021), 174318, https://doi.org/10.1016/j.ejphar.2021.174318.

[44] Q. Zhao, Y. Cheng, Y. Xiong, LTF regulates the immune microenvironment of prostate cancer through JAK/STAT3 pathway, Front. Oncol. 11 (2021), 692117, https://doi.org/10.3389/fonc.2021.692117.

[45] C. Morse, T. Tabib, J. Sembrat, K.L. Buschur, H.T. Bittar, E. Valenzi, Y. Jiang, D.J. Kass, K. Gibson, W. Chen, et al., Proliferating SPP1/MERTK-expressing macrophages in idiopathic pulmonary fibrosis, Eur. Respir. J. 54 (2019), https://doi.org/10.1183/13993003.02441-2018.
[46] J.D. Latoche, A.C. Ufelle, F. Fazzi, K. Ganguly, G.D. Leikauf, C.L. Fattman, Secreted phosphoprotein 1 and sex-specific differences in silica-induced pulmonary fibrosis in mice, Environ. Health Perspect. 124 (2016) 1199–1207, https://doi.org/10.1289/ehp.1510335.
[47] C.A. Brandsma, M. van den Berge, D.S. Postma, M.R. Jonker, S. Brouwer, P.D. Paré, D.D. Sin, Y. Bossé, M. Laviolette, J. Karjalainen, et al., A large lung gene expression study identifying fibulin-5 as a novel player in tissue repair in COPD, Thorax 70 (2015) 21–32, https://doi.org/10.1136/thoraxjnl-2014-205091.
[48] Y. Ruan, Y. Fan, Y. Xie, C. Ma, B. Mo, Y. Lai, G. Li, X. Liu, W. Kuang, Modified Xiaoqinglong decoction alleviates lipopolysaccharide-induced acute lung injury in mice by regulating arachidonic acid metabolism and exerting anti-apoptotic and anti-inflammatory effects, Anat. Rec. 305 (2022) 1672–1681, https://doi.org/10.1002/ar.24822.
[49] M. Shi, W. Deng, E. Bi, K. Mao, Y. Ji, G. Lin, X. Wu, Z. Tao, Z. Li, X. Cai, et al., TRIM30α negatively regulates TLR-mediated NF-κB activation by targeting TAB2 and TAB3 for degradation, Nat. Immunol. 9 (2008) 369–377, https://doi.org/10.1038/ni1577.
[50] M. Wang, H. Zhong, X. Zhang, X. Huang, J. Wang, Z. Li, M. Chen, Z. Xiao, EGCG promotes PRKCA expression to alleviate LPS-induced acute lung injury and inflammatory response, Sci. Rep. 11 (2021), 11014, https://doi.org/10.1038/s41598-021-90398-x.
[51] E. Tsitoura, A. Trachalaki, E. Vasarmidi, S. Mastrodemou, G.A. Margaritopoulos, M. Kokosi, D. Fanidis, A. Galaris, V. Aidinis, E. Renzoni, et al., Collagen 1a1 expression by airway macrophages increases in fibrotic ILDs and is associated with FVC decline and increased mortality, Front. Immunol. 12 (2021), https://doi.org/10.3389/fimmu.2021.645548.
[52] V. Singh, M.I. Khalil, A. De Benedetti, The TLK1/Nek1 axis contributes to mitochondrial integrity and apoptosis prevention via phosphorylation of VDAC1, Cell Cycle 19 (2020) 363–375, https://doi.org/10.1080/15384101.2019.1711317.
[53] M.I. Khalil, C. Madere, I. Ghosh, R.M. Adam, A. De Benedetti, Interaction of TLK1 and AKTIP as a potential regulator of AKT activation in castration-resistant prostate cancer progression, Pathophysiology 28 (2021) 339–354, https://doi.org/10.3390/pathophysiology28030023.
[54] K. Rombouts, T. Mello, F. Liotta, A. Galli, A. Caligiuri, F. Annunziato, M. Pinzani, MARCKS actin-binding capacity mediates actin filament assembly during mitosis in human hepatic stellate cells, Am J Physiol Cell Physiol 303 (2012) C357–C367, https://doi.org/10.1152/ajpcell.00093.2012.
[55] J.H. Buss, L.S. Lenz, L.C. Pereira, D. Torgo, J. Marcolin, K.R. Begnini, G. Lenz, The role of mitosis in generating fitness heterogeneity, J. Cell Sci. 136 (2023), https://doi.org/10.1242/jcs.260103.
[56] W.H. Baricos, S.L. Cortez, S.S. el-Dahr, H.W. Schnaper, ECM degradation by cultured human mesangial cells is mediated by a PA/plasmin/MMP-2 cascade, Kidney Int. 47 (1995) 1039–1047, https://doi.org/10.1038/ki.1995.150.